INTEGRAL

Science Operations Centre

Announcement of Opportunity for Observing Proposals (AO-8)

JEM-X Observer's Manual

INT/OAG/10-0326/Dc

Issue 1.0

15 March 2010

Prepared by E. Kuulkers

Based on inputs from the JEM-X team, DNSC Copenhagen (PI: S. Brandt), and P. Kretschmar, ISOC, ESA/ESAC, Madrid, Spain.

Table of Contents

1 Introduction

The Joint European Monitor for X-rays (JEM-X) on-board INTEGRAL fulfils several roles. It provides complementary data at lower energies (3-35 keV) for the studies of the gamma-ray sources observed by the two main gamma-ray instruments, IBIS and SPI. Normally any gamma-ray source bright enough to be detected by the main instruments will also be bright enough to be rapidly identified with JEM-X. Note, however, that the field of view (FOV) of JEM-X is significantly smaller than those of IBIS and SPI. Flux changes or spectral variability at the lower energies may provide important elements for the interpretation of the gamma-ray data. In addition, JEM-X has a higher angular resolution than the gamma-ray instruments. This helps with the identification of sources in crowded fields. JEM-X can also deliver independent scientific results concerning sources with soft spectra, such as the emergence of new transients or regarding unusual activity in known sources, serendipitously detected in the FOV during the normal observations. Some of these sources may be even not detectable by the other instruments onboard INTEGRAL.

JEM-X operates simultaneously with IBIS and SPI. It is based on the same principle as the two gamma-ray instruments on INTEGRAL: sky imaging using a coded aperture mask. The performance of JEM-X is summarised in Table 1. In Figure 1 the total effective area of JEM-X is shown.

The following Sections give a description of the instrument (Section 2), its operations (Section 3), its performance (section 4), and hints on the use of the instrument (so-called "cook book"; Section 5). For more details, we refer the interested reader to a sequence of papers on the JEM-X payload in the A&A special INTEGRAL issue (2003, Vol. 411, L231-L256). This issue also contains various other papers on the first results from in-flight observations. For a description of the JEM-X data analysis we refer to, e.g., Westergaard et al. (2003, A&A 411, L257). The JEM-X validation report of the **O**ff-line **S**cientific **A**nalysis (OSA) software package released by the ISDC, as well as descriptions of the data analysis pipelines and modules and the use of the OSA software can be found at the ISDC website (http://isdc.unige.ch/?Support+documents).

Table 1: parameters and performance of the JEM-X1 unit

Parameter	**In-orbit value**
Active mask diameter	535 mm
Active detector diameter	250 mm
Distance from mask to detector entrance window	3401 mm
Energy range	3-35 keV
Energy resolution (FWHM)	$\Delta E/E = 0.40 \times [(1/E\ \text{keV})+(1/8\ \text{keV})]^{1/2}$
Angular resolution (FWHM)	3′
Field of view (diameter)	4.8° Fully illuminated 7.5° Half response* 13.2° Zero response
Relative point source location error	1′ (90% confidence radius for a 15σ isolated source)
Continuum sensitivity **for a single JEM-X unit** (isolated source on-axis)	1.2×10^{-4} ph cm^{-2} $s^{-1}keV^{-1}$@ 6 keV 1.0×10^{-4} ph cm^{-2} $s^{-1}keV^{-1}$@ 30 keV for a 3σ continuum detection in a 10^5 s observation with $\Delta E = 0.5E$
Narrow line sensitivity **for a single JEM-X unit** (isolated source on-axis)	2.4×10^{-4} ph cm^{-2} s^{-1}@ 6 keV 1.9×10^{-4} ph cm^{-2} s^{-1}@ 20 keV for a 3σ line detection in a 10^5 s observation
Timing resolution	122 μs (relative timing) ≈1 ms (absolute timing)

* At this angle, the sensitivity is reduced by a factor 2 relative to the on-axis sensitivity. In practice, the transmission of the collimator beyond an off-axis angle of 5° is so low that only the very brightest sources can be observed at larger angles.

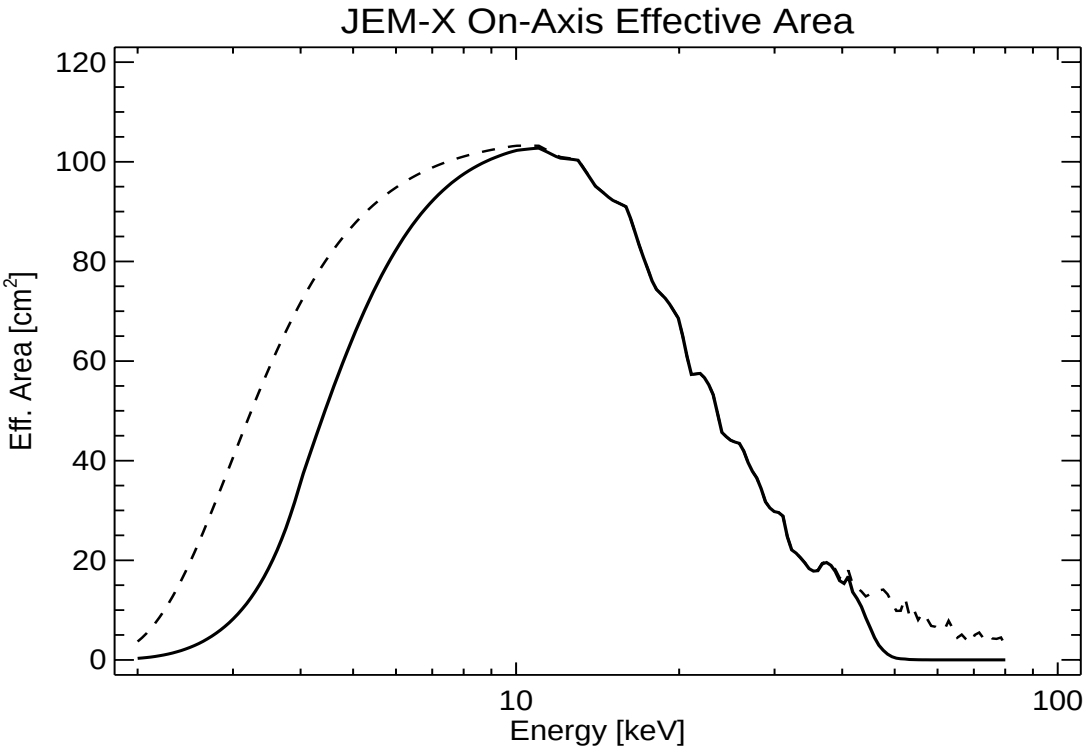

Figure 1: Total effective area of the JEM-X instrument. The dashed curve shows the area before electronic effects are taken into account. The full curve includes the rejection of low signals as well as very high signals.

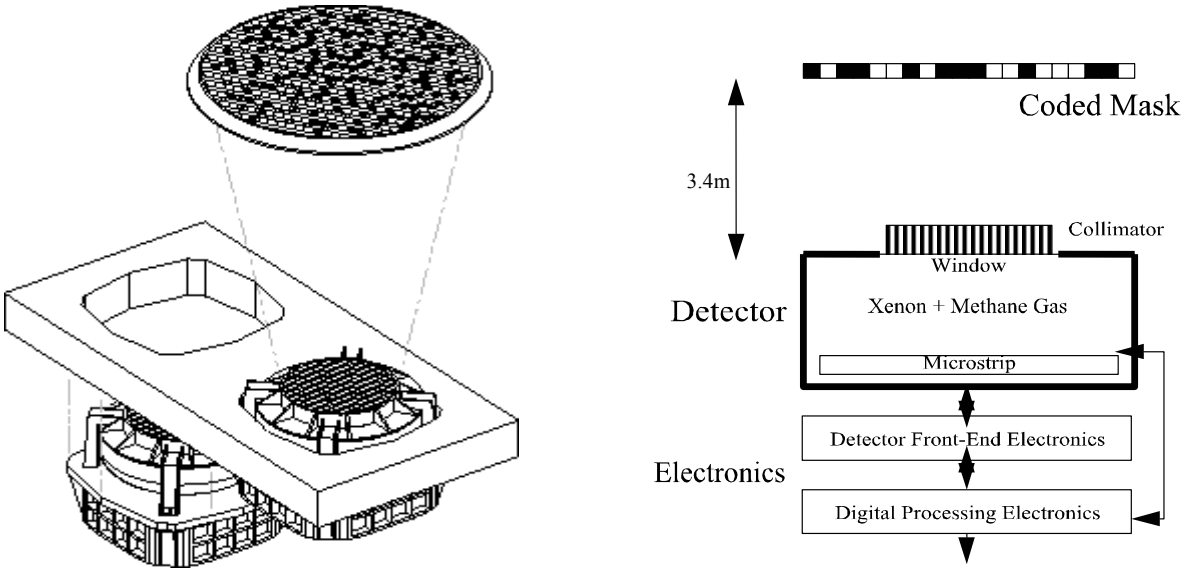

Figure 2: Left: overall design of JEM-X, showing the two units, with only one of the two coded masks. Right: functional diagram of one unit.

2 Description of the instrument

2.1 The overall design and status

JEM-X consists of two identical coded-aperture mask telescopes co-aligned with the other instruments on INTEGRAL. In the current configuration the JEM-X unit "2" is operating while JEM-X "1" is dormant (see also §4). The photon detection system consists of high-pressure imaging Micro-strip Gas Chambers located at a distance of 3.4 m from each coded mask. Figure 2 shows a schematic diagram of one JEM-X unit. A single JEM-X unit comprises three major subsystems: the detector, the associated electronics (see also Figure 6) and the coded mask.

At the end of the Instrument Performance Verification phase, it was decided to operate only one JEM-X unit at a time. The switch-off of one of the units was decided after a gradual loss in sensitivity had been observed in both JEM-X units, due to the erosion of the micro-strip anodes inside the detector. By lowering the operating voltage, and thereby the gain of the detectors, the anode damage rate has now been reduced to a level where the survival rate of the detectors seems to be assured for the extended mission phase. The dead anodes with permanently low or no activity are taken into account in the OSA analysis software. If, in the future, both units are to be switched on together again, the total sensitivity will increase by approximately a factor $\sqrt{2}$. However, at the time of writing of this document, such a change has not being considered.

2.2 The detector

The JEM-X detector is a micro-strip gas chamber with a sensitive geometric area of ~500 cm^2 per unit. The gas filling is a mixture of xenon (90%) and methane (10%) at 1.5 bar pressure. The incoming photons are absorbed in the xenon gas by photo-electric absorption and the resulting ionisation cloud is then amplified in an "avalanche" of ionisations by the strong electric field near the micro-strip anodes. Significant electric charge is picked up on the strip as an electric impulse. The position of the electron avalanche in the direction perpendicular to the strip pattern is measured from the centroid of the avalanche charge. The orthogonal coordinate of an event is obtained from a set of electrodes deposited on the rear surface.

Hotspots appear from time to time on the detector micro-strip plate. They are weak except at very low energies (<2.5 keV) where their peak intensity can be high (up to 100 cts/s), but they last only minutes, at most hours, not days. Their physical extent is a few mm^2. They are identified in the OSA analysis software in the data correction step and are consequently excluded from further analysis. So far, there are no "hot strips" detected.

The X-ray window of the detector is composed of a thin (250 μm) beryllium foil which is impermeable to the detector gas but allows a good transmission of low-energy X-rays.

A collimator structure with square-shaped cells is placed on top of the detector entrance window. It gives support to the window against the internal pressure and, at the same time, limits and defines the field of view of the detector. It has an 85% on-axis transparency. The collimator is important for reducing the count rate caused by the cosmic diffuse X-ray background. However, the presence of the collimator also means that sources near the edge of the field of view will be attenuated with respect to on-axis sources (see Figure 3). The materials for the collimator (molybdenum, copper, aluminium) have been selected in order to minimise the detector background caused by K fluorescence.

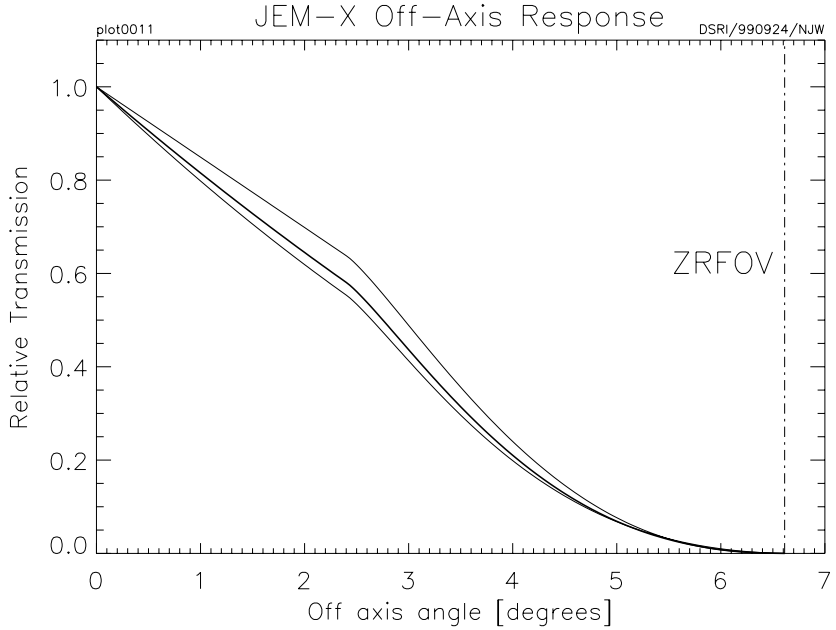

Figure 3: Off-axis response of JEM-X. The middle curve shows the average transmission through the collimator, including all azimuth angles.

Four radio-active sources are embedded in each detector collimator in order to calibrate the energy response of the JEM-X detectors in orbit. Each source illuminates a well defined spot on the micro-strip plate. The gain of the detector gas is monitored continuously with the help of these sources. Figure 4 shows the collimator layout and the locations of the calibration sources.

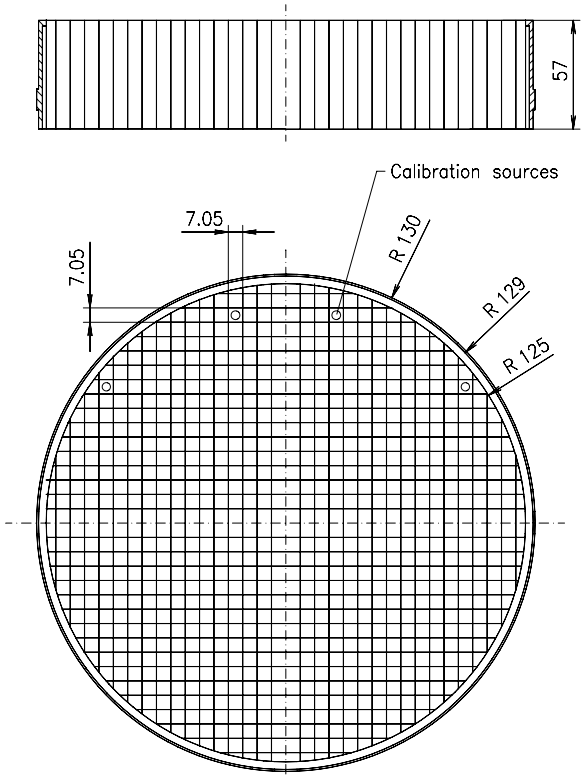

Figure 4: Collimator layout. In this diagram the 4 calibration sources are situated on the upper side. The dimensions are in mm, i.e., collimator height = 57 mm and radius = 130 mm.

2.3 The coded mask

The mask is based on a Hexagonal Uniformly Redundant Array (HURA). For JEM-X, a pattern composed of 22501 elements with only 25% open area has been chosen. The 25% transparency mask actually achieves better sensitivity than a 50% mask, particularly in complex fields with many sources, or in fields where weak sources should be studied in the presence of a strong source. A mask with lower transparency also has the advantage of reducing the number of events to be transmitted, while at the same time increasing

the information content of the remaining events. Considering the telemetry allocation to JEM-X, this means an improved overall performance for the instrument, particularly for observations in the plane of the Galaxy.

The JEM-X imaging is affected by some (limited) coding noise, but does not suffer from "ghost" images, except in rare cases, because the pattern of the mask only repeats itself near the edges of the mask.

The mask height above the detector (~3.4 m) and the hexagonal mask element dimension (3.3 mm centre-to-centre) define together the angular resolution of the instrument, in this case: 3′. Figure 5 illustrates the JEM-X coded mask pattern.

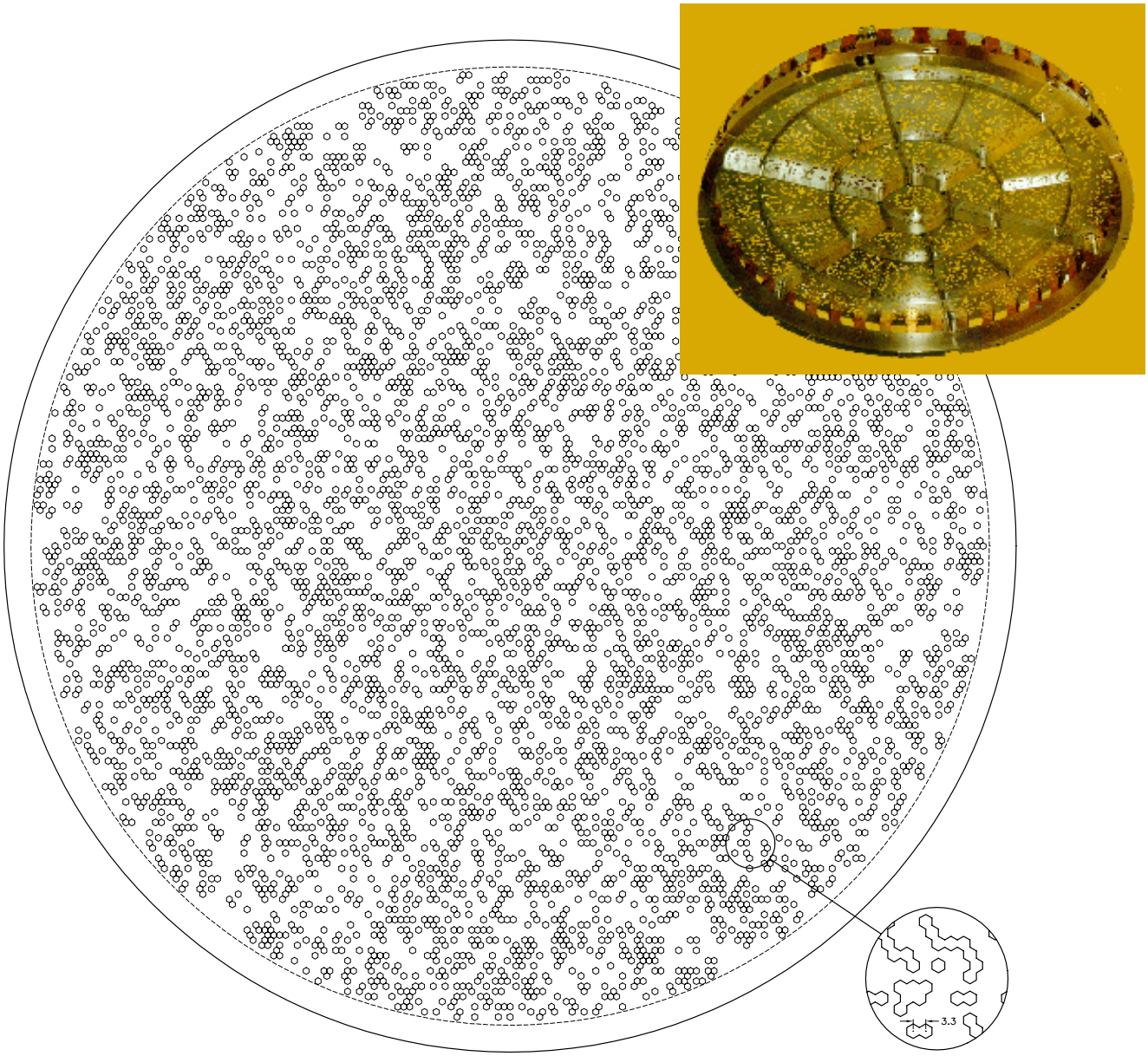

Figure 5: Illustration of the JEM-X coded mask pattern layout without the mechanical interface. The diameter of the coded mask is 535 mm. The mask has a transparency of 25%. A picture of the mask is shown at the top right.

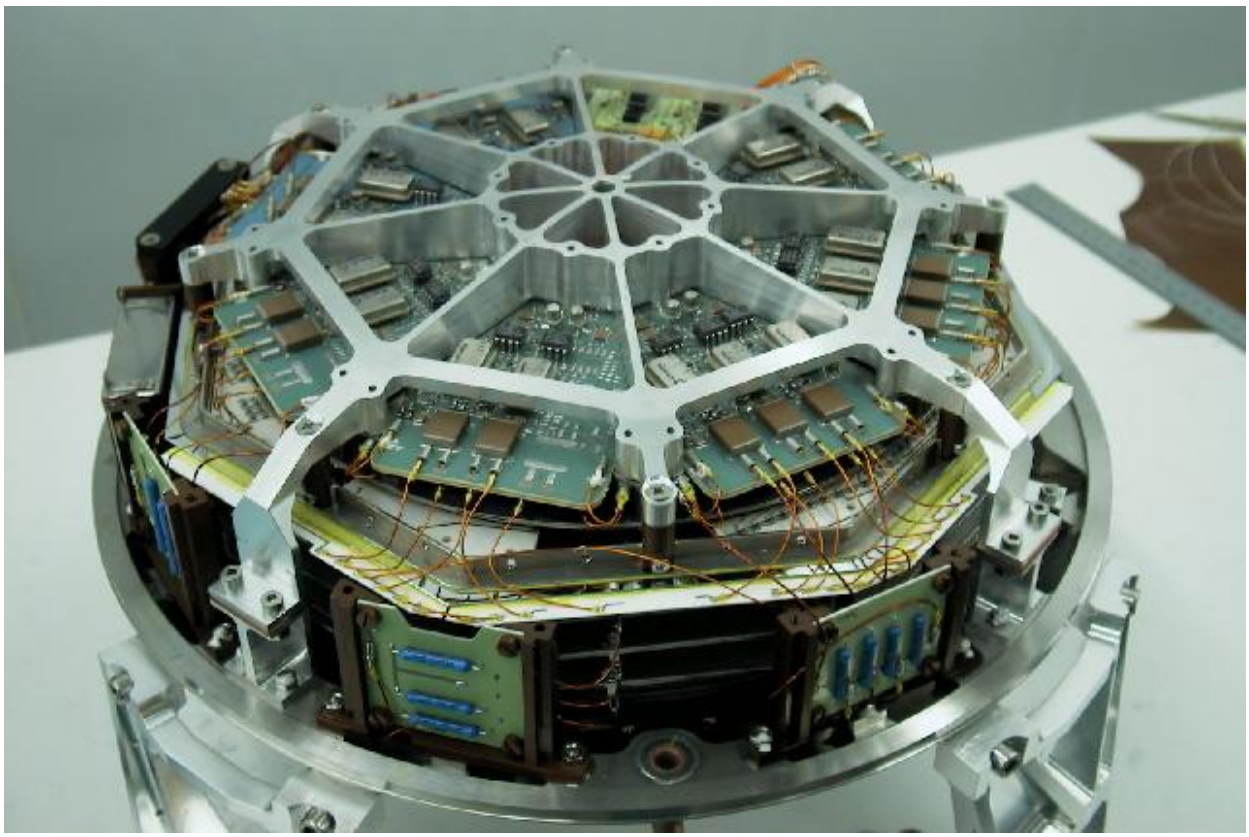

Figure 6: JEM-X Qualification Model detector during assembly.

3 Instrument operations

3.1 Telemetry formats and their use

In order to make the best of a situation with a limited telemetry band-width, two types of on-board data reduction can in principle take place for the JEM-X instruments:

1) A grey filter can randomly remove *some of the events* from the telemetry data stream. This takes place automatically when the telemetry buffer fills up beyond a certain limit and will typically happen for JEM-X count rates higher than about 90 counts/s including background, or ~500 mCrab, at standard telemetry allocation.
2) The on-board software can switch to a "reduced event" telemetry format which removes *part of the information* about each event from the telemetry data stream. For each observation, two formats, "primary" and "secondary" can be defined. Observations will begin in the "primary" format and can switch to the "secondary", if the current count rate is too high – and switch back if the possibly higher transmission rate is no longer required.

In practice, all data formats except for the "Full Imaging" default format suffer various shortcomings – e.g., lack of spatial gain corrections due to the lack of positional data or very limited support within the OSA software – that make them of little use to general observers. Therefore, the telemetry format can not be chosen by the user in the Proposal Generation Tool (PGT), but is pre-set to "Full Imaging" for primary and secondary format on-board.

In the unlikely case that a specific observation requires the use of another telemetry format than "Full Imaging", the observer needs to specify and justify this fact in the scientific justification. If the proposal is accepted, ISOC would then set the required modes before scheduling the proposal.

3.2 The grey-filter mechanism

The grey-filter process can operate with 32 different transmission fractions. These fractions are 1/32, 2/32, …, 31/32, 32/32. The filter values to be used will be chosen by the instrument electronics during the actual observation, taking into account the total background count rates. The grey filter will always be adjusted automatically by the on-board software to match the data stream to the available telemetry capacity, thus the term "automatic grey filter". Whenever the grey filter level is changed (decreased or increased) the on-board software checks whether a telemetry format change should also take place – in the default set-up (see above), this has no effect, as the "Full Imaging" format is used throughout.

3.3 TM buffer flushing

The JEM-X instruments have an internal buffer capable of storing up to 60000 events. This allows JEM-X to accommodate temporary count rate increases without data loss. But if the telemetry allocation averaged over a science window does not allow transmitting all events, then those events which remain in the on-board buffer when a new observation starts, will be flushed and lost.

3.4 Detailed overview of the telemetry formats

The following information is given for reference only, as the "Full Imaging" format is the only format that has been calibrated and fully supported by the OSA analysis software.

Table 2: Characteristics of the JEM-X Telemetry Formats.

Format Name	Detector Image Resolution (pixels)	Timing Resolution	Number of Spectral Channels	Event rate (cps) until onset of grey filter
Full Imaging	**256 x 256**	**1/8192s = 122μs**	**256**	**70**
Restricted Imaging	*256 x 256*	*1/8 s = 125 ms*	*8*	*270*
Spectral Timing	*None*	*1/8192s = 122μs*	*256*	*180*
Timing	*None*	*1/8192s = 122μs*	*None*	*500*
Spectrum	*None*	*1/8s = 125 ms*	*64*	*2000*

4 Performance of the instrument

JEM-X currently operates with one active and one dormant unit. The impact operating one or the other, instead in parallel, is a smaller total sensitive area, but the expected total lifetime has increased. The nominal telemetry allocation is 7 science packets and 1 housekeeping packet per 8 seconds for the active unit. This allows to transmit about 90 counts/s before events will begin to pile up in the onboard buffer – this will eventually force the grey filter mechanism to set in (90 counts/s corresponds to about the count rate for a ~500 mCrab source plus the solar minimum instrumental background). At the beginning of a new pointing (so-called "science window") the grey filter is set to full transmission, and therefore, even for higher count rates there will always be a period in the beginning of every pointing where all data are transmitted – the catch is that some of the data taken at the end of the pointing may be lost as the onboard buffers are flushed when the following pointing begins.

4.1 Background

The JEM-X background during solar minimum conditions has been measured from a number of empty field observations. The background rate currently is about 35 counts/s in the 3 to 35 keV range, when the spacecraft is outside the radiation belts. Figure 7 shows a background spectrum from JEM-X 2, averaged over 46 science windows in August 2008 (revolution 716).

The background radiation environment is mainly produced by two components: the diffuse X-ray background and the X- and gamma-radiation induced by cosmic rays. The diffuse X-ray background dominates the background below about 15 keV and the cosmic ray induced background dominates at higher energies. The line at about 30 keV is due to fluorescence photons from the Xenon gas in the volumes surrounding the active detector volume. It is a useful calibration line and an indicator of the effective resolution of the instrument.

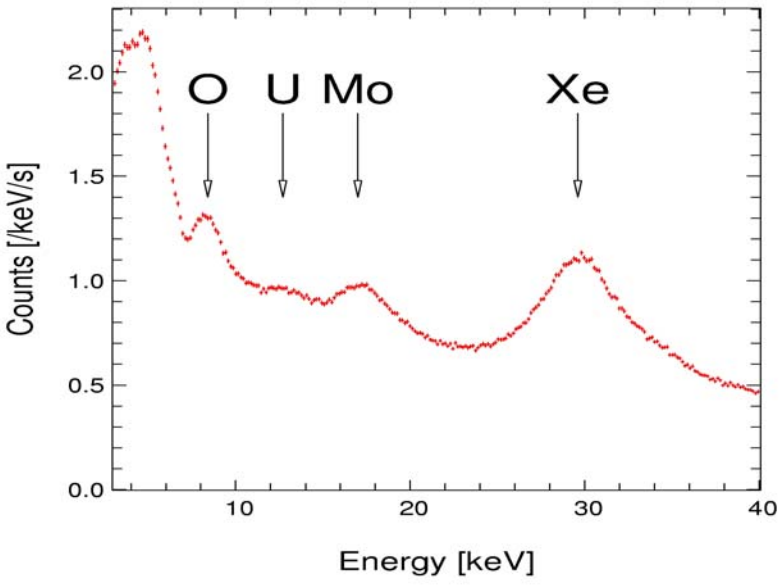

Figure 7: Full JEM-X 2 detector spectrum of empty field observations with diffuse and instrumental background. The most significant fluorescent lines are indicated (the uranium is from contamination in the Be-window).

There are other instrumental lines visible as well. The background increases noticeably at the edge of the detector which is why the useful detector diameter is only 220 mm, rather than the 250 mm physical diameter. Tthe useful diameter depends on the chosen energy range because the background distribution is strongly energy dependent. The rejection of background events produced by charged particles crossing the detector is accomplished with a combination of pulse

height, pulse shape and "footprint"-evaluation techniques. These techniques reach a particle rejection efficiency better than the 99.5% level.

4.2 Timing stability and resolution; dead-time

JEM-X observations of the Crab pulsar have shown that the absolute timing is stable to better than 100 μs. The individual JEM-X counts are binned into time bins with a width of 122 μs. However, the Crab analysis shows that the phase of the timing bins is stable within a few μs.

The dead-time depends on the event rate and telemetry format used. It is automatically taken care of in the OSA analysis software.

4.3 Imaging: resolution and detection limits

The accuracy of source position determinations depends on the number of sources, background counts and on the off-axis angle of the source. Analysis of the standard JEM-X images show that the point spread function of JEM-X is well represented by a symmetrical 2D Gaussian function with a standard deviation of 1.2′. This resolution defines the JEM-X ability to check for the presence of multiple sources, and also the ability to separate spectra from two sources at small angular separations.

The source positions are best determined when sources are observed on-axis. The JEM-X vignetting function has the shape of a pyramid, so even within the central "fully illuminated" region the instrument response varies significantly between different off axis positions.

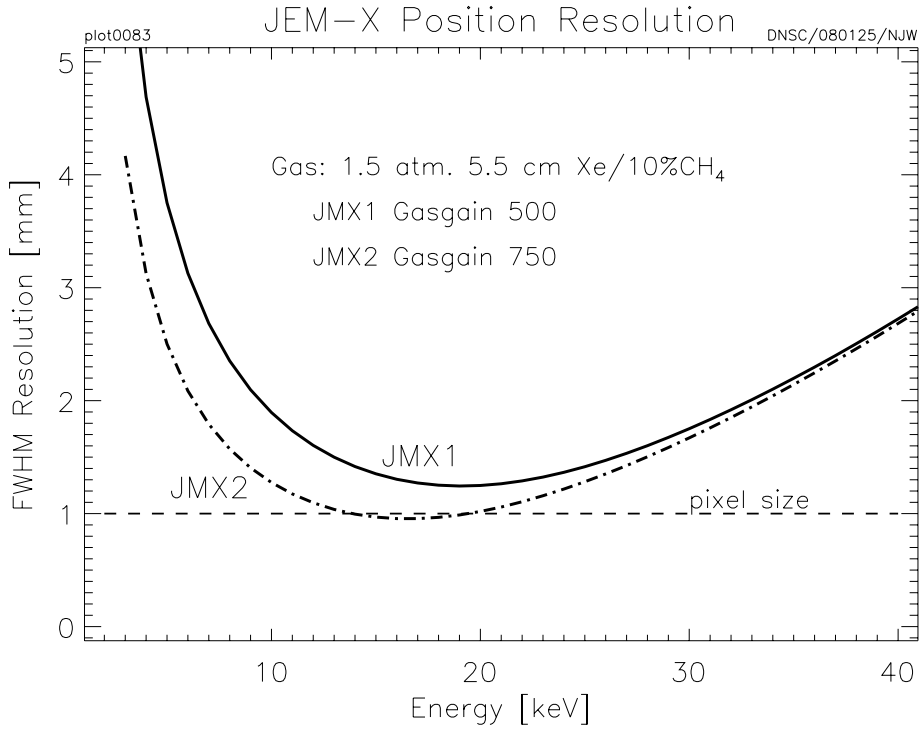

Figure 8: The positional resolution in the JEM-X1 and JEM-X2 detectors as a function of energy. Note that the positions are rounded to 1 mm accuracy in the down-linked data.

The intrinsic detector position resolution is shown as function of energy in Figure 8 for photons entering on-axis. The degradation below 10 keV is caused by the electronic noise of the front-end amplifiers; above 10 keV it is caused by the increase of the primary photo-electron range with energy. The intrinsic positional resolution of the detector is finer than the pixel size of the coded mask (3.3 mm) over most of the energy range. The determination of the photon positions in the image plane is affected by parallax for higher energy photons entering at off-axis angles. This effect is not of prime importance for source positioning, but the smearing of the image affects the off-axis sensitivity at energies above 20 keV.

The alignment of the detector with respect to the INTEGRAL star tracker appears to be stable to better than 5 arcseconds and the star tracker accuracy is even better than this. The JEM-X OSA8 software yields source positions to better than 10" provided the detection significance is high.

The source detection limit for single science windows also depends on the background conditions and on the off-axis angle of the source. However, 20 mCrab sources are reliably detected under normal background conditions if they appear at less than 3 degrees off-axis. Better sensitivities can be obtained by "mosaicking" overlapping images from several science windows. A deep mosaic image example is shown in Figure 9, while Figure 10 and Figure 11 illustrate the source detection capabilities obtained from mosaic images as a function of effective accumulated observation time (corrected for dead time, grey filter and vignetting effects).

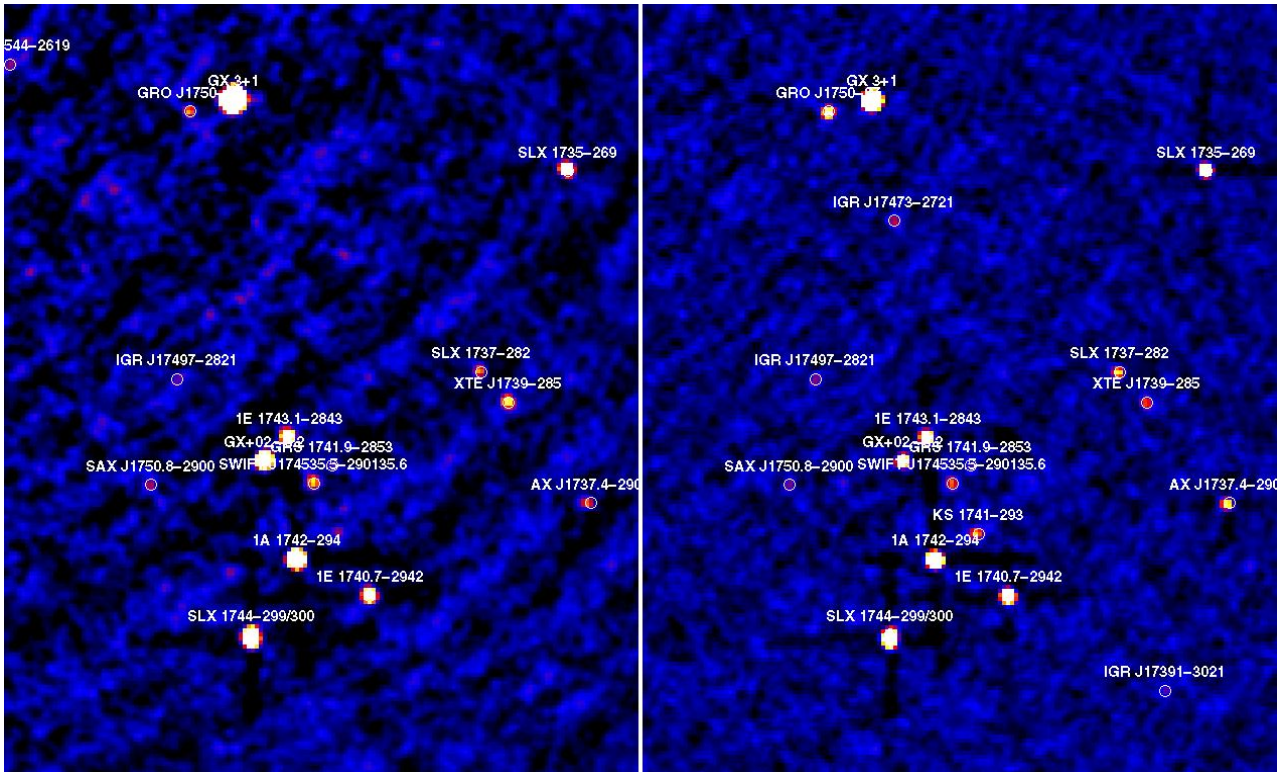

Figure 9: Deep mosaic significance image of the region around the Galactic bulge, based on over 3000 JEM-X exposures (science windows) in the 3-10 keV (left) and 10-25 keV (right) energy bands. The effective exposure at the centre is close to 3 Msec; the field is about 4°x5° wide. Persistent and transient sources are annotated in white and red, respectively. Note that not all the sources in the Galactic Center region (middle) have been annotated.

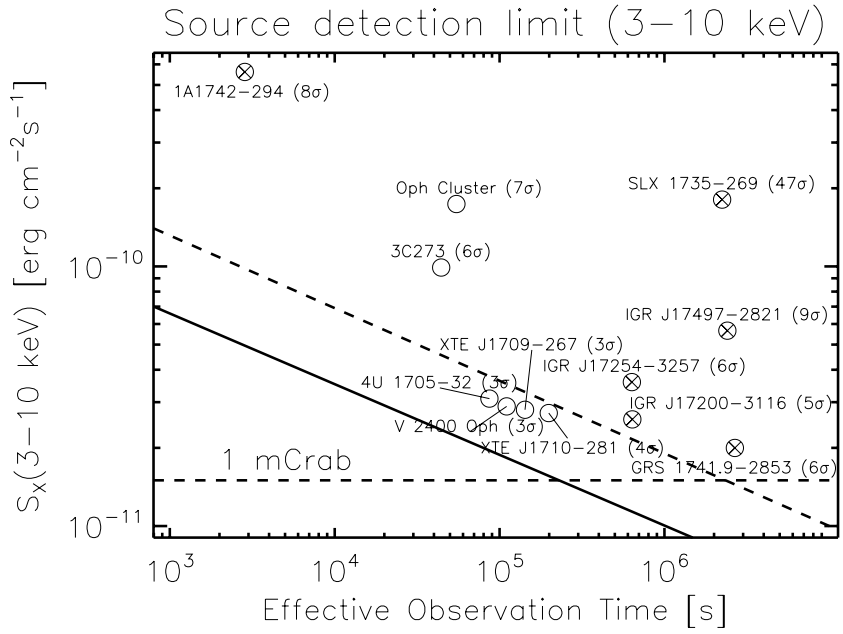

Figure 10: Source detection capabilities in the 3-10 keV energy band as a function of the effective accumulated exposure time in JEM-X mosaic images corrected for dead time, grey filter and vignetting effects. The slope of the lines is obtained from simulations where an isolated source must be detected at 6σ in the deconvolved image. The dashed line represents the case where there are additional sources in the field of view giving a background corresponding to a total of 1 Crab. The positions of the lines are determined by actual measurements. Examples of such actual observations are given: the source 3C 273 and the other empty circles are instances of isolated sources, while the crossed circles represent sources observed in the crowded Galactic Centre region. The σ values given in parentheses are obtained from a measure of the highest source pixel in significance mosaic maps with the default pixel size (1.5').

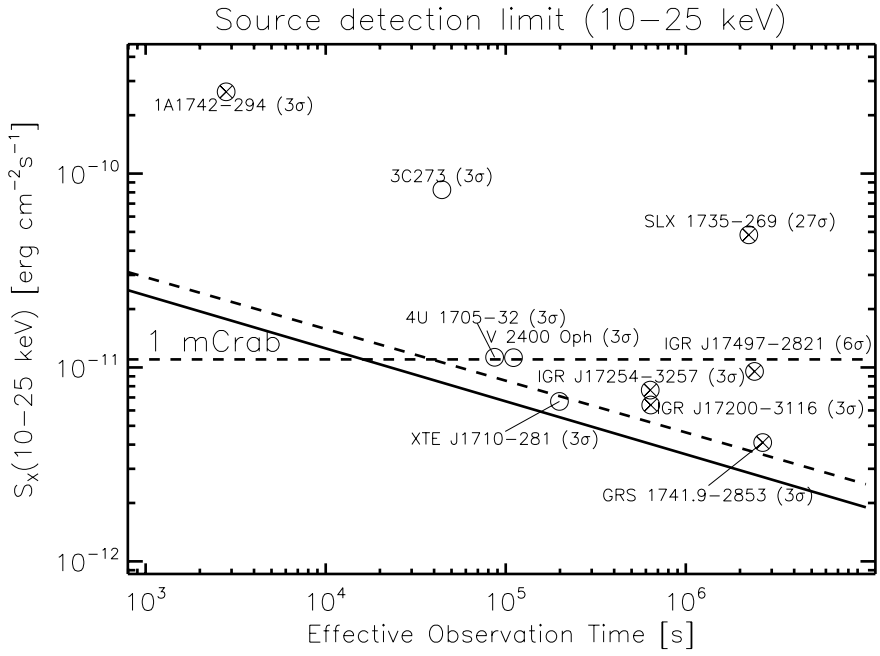

Figure 11: Same as Figure 10, but for the energy range from 10 to 25 keV.

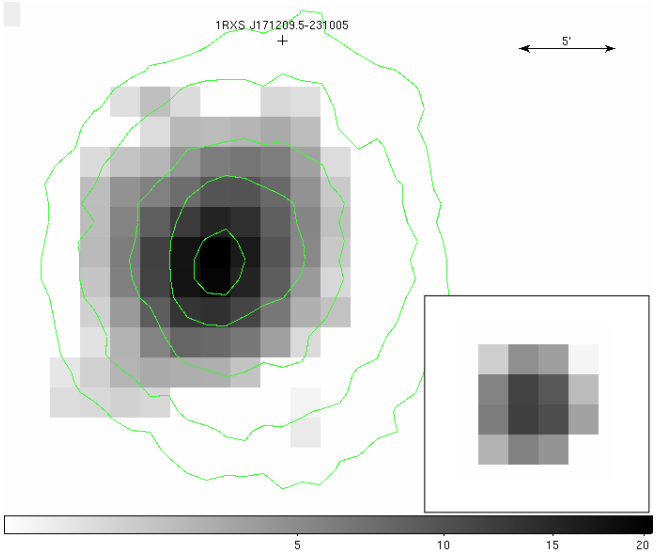

Figure 12: JEM-X significance image of the Ophiuchus cluster in the 3-18 KeV band, with the surface brightness contours from ASCA overlayed. The inset shows the image of a known point source (V2400 Oph, a cataclysmic variable) in the same field, demonstrating the extended nature of the cluster. The cross shows the position of 1RXS J171209.5-231005, the nearest known X-ray point source. (From Eckert et al. 2008, A&A 479, 27)

JEM-X's good spatial resolution makes it possible to analyse also extended sources. An example is the Ophiuchus cluster, which is bright in the X-ray region. A JEM-X significance image is shown in Figure 12. Clearly, the cluster emission is extended; the angular size of the X-ray source at half-maximum is 3.2', and therefore the morphology can be investigated.

4.4 Detector energy resolution

The energy resolution of the JEM-X instruments slowly degrades with time when the instruments are used. This is the primary reason why only one JEM-X unit is used at a time (see Section 2.1). Two effects have been noted to change over time: one is an increase in the recovery time for local modifications (drops) in the gas amplification following large charge deposits on the micro-strip plate caused by the passage of heavy cosmic rays. The second effect is a gradual change (increase) of the gas amplification for a constant detector voltage. This change is not the same everywhere on the detector, and requires remapping the gain map using the xenon fluorescence line from time to time. Physically, the degradation is suspected to be caused by gradual changes in the conductivity of the micro-strip glass substrate due to ion migration. The JEM-X team generates regular updates to the response files to be used with the OSA, in order to take into account this evolution.

The degradation of the energy resolution is most noticeable at the highest energies. It can be described by an additional, slowly time-varying, term in the following equation:

$$\Delta E/E = 0.4 \times [(1 / E\ [keV]) + (1 / E_{noise}\ [keV])]^{1/2}.$$

E_{noise} can be interpreted as the energy where the resolution has degraded by a factor $\sqrt{2}$. For JEM-X2, E_{noise} is currently close to 8 keV. In-flight calibration work is ongoing that might lead to a higher value of E_{noise}.

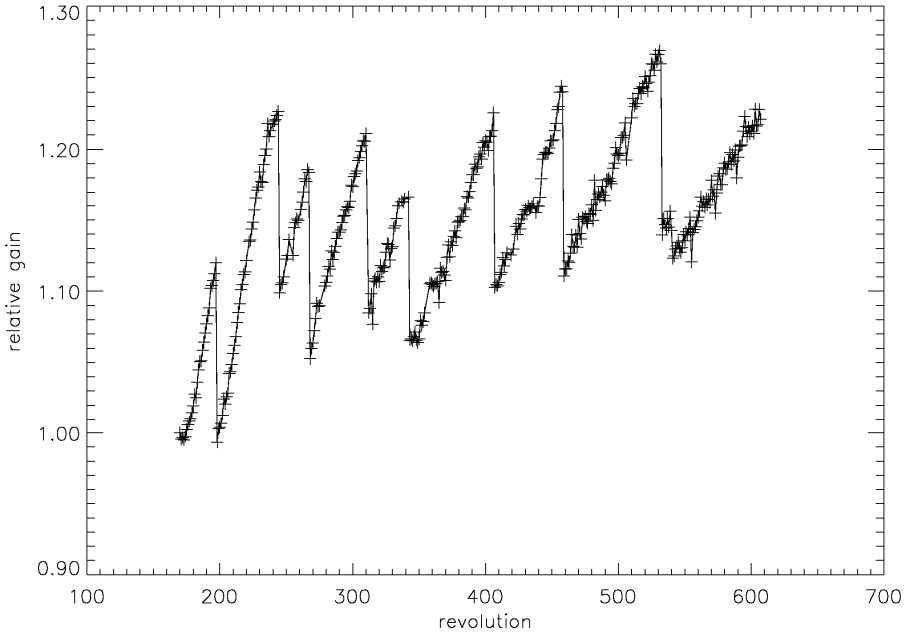

Figure 13: Average gain per orbit for JEM-X1 normalized to the gain of revolution 170. The average has been adjusted for a temperature dependent gain variation to show the overall trend of gain increase over time. The steps in gain correspond to the lowering of the high voltage setting. A similar development is expected for JEM-X2 where the cathode voltage is adjusted so that the gain remains within +/-10% (disregarding temperature effects that may add or subtract about 5%). The effect of the changing gain is taken care of in the OSA8 software.

4.5 Detector gain

There are four radio-active calibration sources in each of the JEM-X detectors. JEM-X1 has two Cd-109 and two Fe-55 radiating at 22 keV and 5.9 keV, respectively. JEM-X2 has all four calibration sources with Cd-109. The detector gain is monitored continuously by the counts from these sources. The gain of the JEM-X detectors has been found to increase slowly over time. By lowering the high voltage at suitable times the gain is confined to a limited band (see Figure 13). On top of this, the gain is also dependent on the detector temperature (currently about 3% change per ºC), but all of this is automatically corrected for in the analysis correction level.

4.6 Spectral analysis

For bright sources, spectra can be extracted in a straightforward manner using the spectrum extraction step of the OSA software. An example is given below in Figure 14 for the Crab. This gets more problematic for weak sources in crowded fields, where contamination from the brighter sources affects results. In these cases, extracting spectra from mosaic images is recommended. An example is given in Figure 15 for IGR J17254-325, a source of ~2 mCrab in the 3-10 keV band, surrounded by brighter sources. For more detailed information about the extraction of spectra, we refer to the ISDC's JEM-X User Analysis Manual available from http://isdc.unige.ch/?Support+documents.

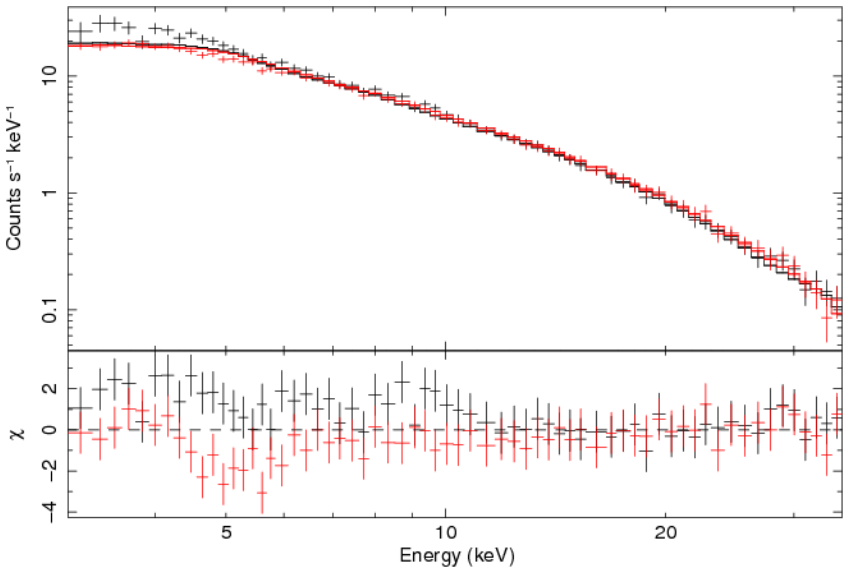

Figure 14: JEM-X1 (black) and JEM-X2 (red) Crab count spectra together with the simultaneous fit to a power-law emission model, $dN/dE=N(E/1\ keV)^{-\Gamma}$ ph cm^{-2} s^{-1} keV^{-1}, subjected to photo-electric absorption of $0.36x10^{22}$ atoms cm^{-2}, with N is 6.65 and Γ is 2.0. The data are from revolution 39 with a total exposure time of 1.2 ksec. A systematic error of 3% has been added. The goodness-of-fit is $\chi^2=149$ for 126 degrees of freedom.

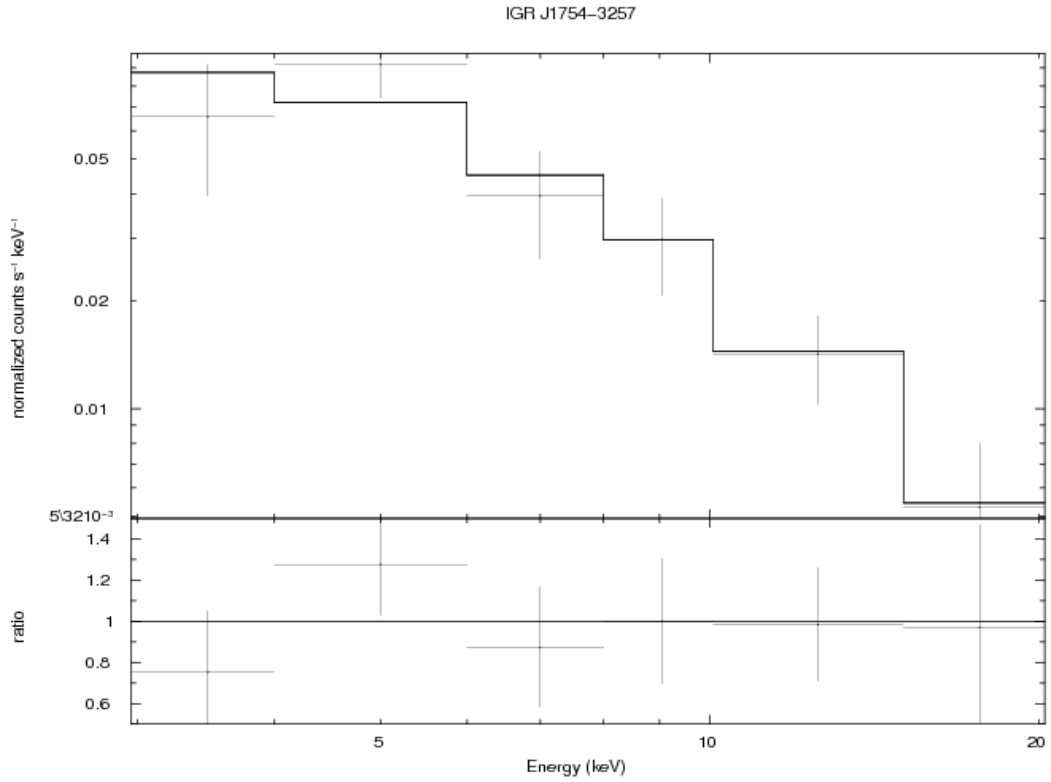

Figure 15: JEM-X spectrum of IGR J17254-3257, obtained from mosaic images with a total of ~310 ksec exposure. The spectral fit shown is a simple power law.

4.7 X-ray burst detection

X-ray bursts can be searched for using JEM-X detector light curves with typically ~10 s time bins. In order to verify that a burst found in the detector light curve really comes from a point source, an image must be generated with an exposure time corresponding to the time interval of the burst, and then be compared to a corresponding image covering an equivalent interval before or after the burst. Once a point source origin has been verified, the source light curve and spectrum can be extracted and investigated for the burst characteristics. As an example, we use the detection with JEM-X of the first observed X-ray burst from the source IGR J17254-3257 on February 17, 2004 (Brandt et al., ATel #778).

Figure 16 shows the detector light curve (in black) together with IGR J17254-3257 source light curve (in red) both in the 3-10 keV energy band, with 10 s time bins in a 6 minute time interval. One can actually see on the detector light curve another stronger burst from the source 1A 1742-294 occurring less than one minute after the former. The source light curve, which is vignetting corrected, shows that the IGR J17254-3257 burst peak is much more pronounced than in the detector light curve.

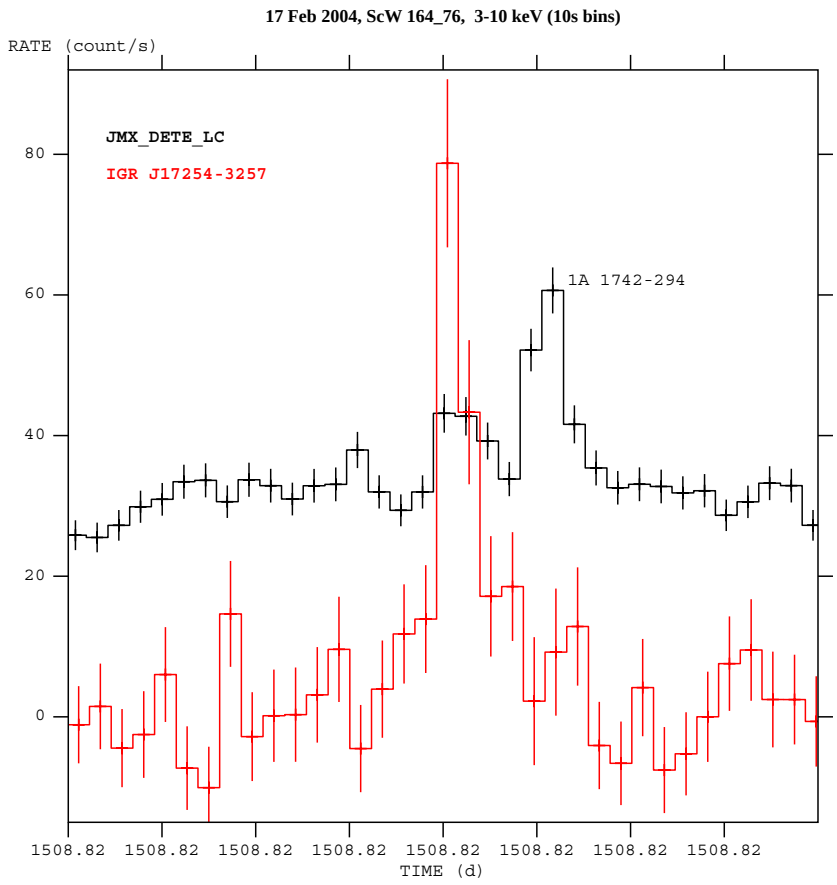

Figure 16: JEM-X detector light curve (black) and IGR J17254-3257 source light curve (red) during a 6 minute interval around the burst that occurred at UTC 19:44:00 on 17 February 2004. Note that another, stronger, burst from 1A 1742-294 occurred less than one minute after the event from IGR J17254-3257.

Figure 17 shows the 45 s exposure taken during the burst (left) where only IGR J17254-3257 is visible and the whole science window exposure (right) where a number of other sources are also visible, but not IGR J17254-3257, due to its very low persistent emission. A zoom around the position of IGR J17254-3257 is also displayed in each case.

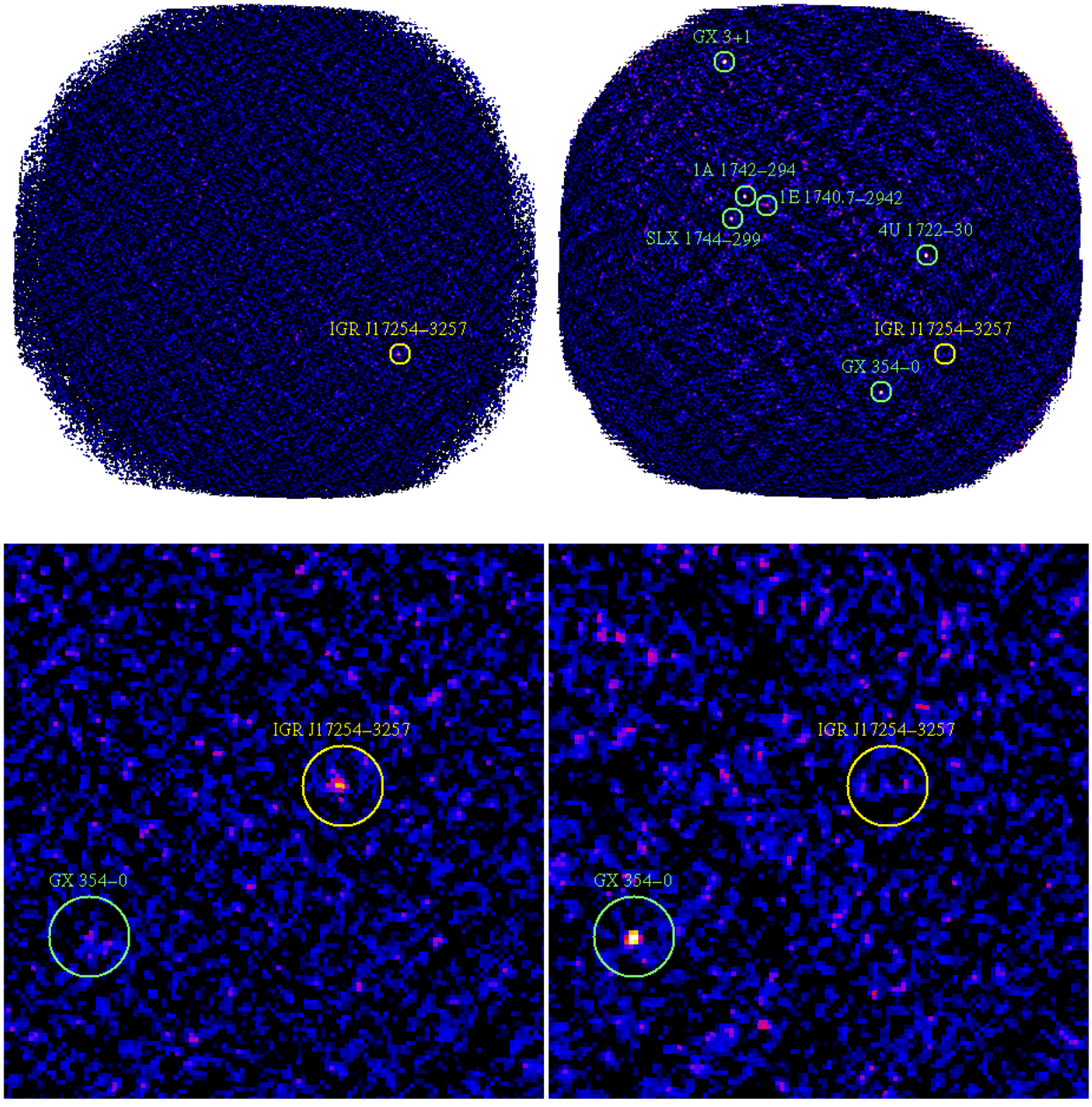

Figure 17: JEM-X 3-10 keV images obtained during a 45 s exposure around the X-ray burst from IGR J17254-3257 (left) and over the whole science window (right).

5 Observation "cook book"

5.1 Considerations of the use of the instrument

The primary role of JEM-X is to provide simultaneous data on the X-ray flux and variability of the targets observed by the two main gamma-ray instruments IBIS and SPI. JEM-X can often pinpoint the source positions with a better precision than IBIS and is thus capable of contributing to the identification of new sources.

The sensitivity of a coded mask instrument like JEM-X is critically dependent on the software used to analyse the data - much more so than for simpler types of X-ray instruments. The sensitivity examples mentioned below should therefore not be considered as final. Improvements in the spectrum extraction software are expected, which may increase the S/N. Likewise, specific user choices during the data analysis can reduce the effective area to be used for a given JEM-X data set. This can lead to the necessity of using constant offsets when doing simultaneous spectral fitting of JEM-X spectra together with other spectra from the other instruments.

Users should also be aware that the current spectral extraction and vignetting corrections for sources with off-axis angles greater than 3 or 4 degrees should be interpreted with caution.

Concerning the source detectability, it can be noted that during exposures of typically 2000s, practice has shown that sources down to about 6 mCrab and 8 mCrab (between 3-10 keV and 10-25 keV, respectively) are found if they are within the central few degrees of the field of view. These numbers refer to observations with a single JEM-X unit.

5.2 Loss of JEM-X sensitivity due to 5x5 dithering

Most INTEGRAL observations are done using a 5x5 dither pattern with points spaced 2.17° apart. Dithering is necessary for SPI and recommended for IBIS. Unfortunately, such dithering does not allow JEM-X to observe the target source continuously. In the 5x5 mode, only the central 9 out of the 25 dither pointings yield useful JEM-X spectral data for the central source. The target is simply too far off-axis during the remaining 16 dither points (see also Figure 3, page 9). Table 5 shows the average degradation for the different spacecraft dithering patterns. When the JEM-X coverage is an integral part of the observation, the hexagonal dither pattern may be selected ("staring" is not recommended).

To further reduce systematic effects in deep mosaic images of IBIS/ISGRI, an offset between the centre of each dither (either 5x5 or hexagonal) cycle was introduced in AO3 for observations requiring several dither cycles. This ensures that no pointing attitude is repeated over the course of the observation. Hence, the **C**entre **O**f a dither **P**attern (COP) moves around in a pattern during an observation (see the document ***Overview, Policies and Procedures***). With the COP move, the imaging noise in the JEM-X mosaic images has also been reduced. Additionally, a sequential rotation covering the range +/-3 degrees between successive repetitions of the same (5x5) pattern has been implemented by ISOC in AO5 (see again the document ***Overview, Policies and Procedures***).

Table 3: Effective JEM-X observation times for different dithering modes.

Dithering mode	Effective observation time
Staring	100%
Hexagonal dither	69%
''5 × 5'' dither	23%

5.3 How to estimate observing times

This section describes how to estimate observing times in order to detect X-ray continuum emission and line emission with JEM-X. It is assumed that there is *no dithering* (i.e. "staring" mode) and that only one JEM-X unit is used. The instrument sensitivities quoted here are basically the same as in previous AO's.

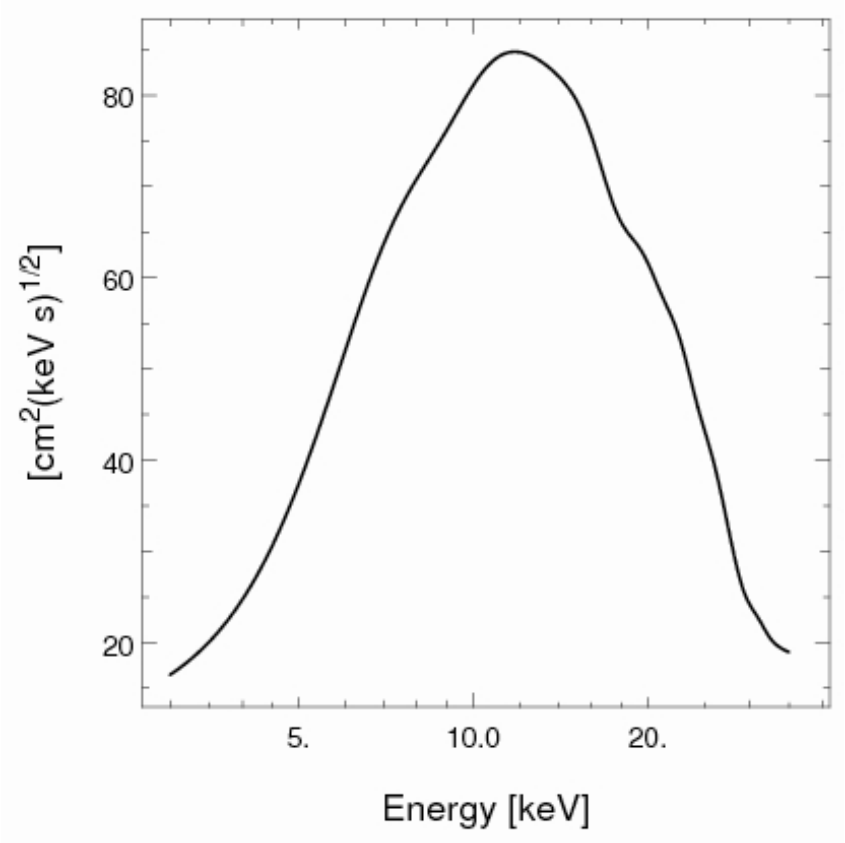

Figure 18: C-factor for estimating the continuum sensitivity for the JEM-X 2 unit (see formula in Section 5.4).

5.4 Continuum emission

In Figure 18 the factor *C(E)* is shown. In order to estimate the continuum sensitivity for various detection levels (N_σ = number of sigmas) and observation times t_{obs} (s), the C-factor can be used together with the following equation:

$$N_\sigma = F_{cont}(E) \times \sqrt{\Delta E \times t_{obs}} \times C(E),$$

where $F_{cont}(E)$ is the continuum flux (photons cm^{-2} s^{-1} keV^{-1}) and ΔE the energy resolution (keV).

5.5 Practical examples

This Section gives some practical examples which illustrate the use of the formula described in the previous section. To conclude, Table 4 lists the actual JEM-X background count rates for a single JEM-X unit as well as the observed count rates for the Crab (Nebula and pulsar) on-axis, as measured in-orbit.

Table 4: Count rates for a single JEM-X unit (Crab on-axis).

Interval [keV]	**Crab counts s^{-1}**	**Diffuse X-ray Background counts s^{-1}**	**Cosmic Ray induced counts s^{-1}**	**Total bkg counts s^{-1}**
3 - 10	83	2.7	5.0	7.7
10 - 20	27	1.7	5.4	7.1
20 - 35	5.4	0.5	8.5	8.9
Total: 3 - 35	115	4.9	18.8	23.7

5.5.1 Continuum studies

Consider a 10 mCrab (3-10 keV)[†] AGN with a photon spectral index of 1.7. How much observation time is needed for a continuum detection at various energies?

Assume a staring on-axis observation, i.e., with no sensitivity loss due to dithering and no other strong sources in the field of view. We can then estimate the time needed to get a 5σ detection in a prescribed energy band. Table 5 shows the result at three selected energies and energy bands.

Table 5: JEM-X continuum sensitivity study

E(keV)	ΔE(keV)	Flux (photons $cm^{-2}s^{-1}keV^{-1}$)	C(E)	Required Exposure Time (s)
4	2	4.6×10^{-3}	25	945
10	4	9.7×10^{-4}	82	990
20	6	3.0×10^{-4}	62	12000

5.5.2 Comparing 5x5 dither and hexagonal dither

The usual observation mode of INTEGRAL is shifting the boresight in a dither pattern, most often a 5x5 pattern with a step size of 2.17 degrees. A hexagonal pattern (7 pointings) with an offset of 2.0 degrees is also an option.

Figure 3 (page 9) shows the throughput fraction as a function of off-axis angle; the right hand side of the expression for N_σ in Section 5.4 must be expanded to include this fraction as a factor as well.

Take an observation of a 30 mCrab source in a 5x5 dither where the total observation time is 90 ks (an hour per pointing), as given in Table 6. The combination of these observations gives N_σ = 14.8. If the same observation time is spent in a hexagonal dither, then the numbers come out as given in the lower part of the table and the combined observations yield N_σ = 27.2.

Table 6: JEM-X dither sensitivities

Off-axis (deg)	Time (ks)	N_σ
90 ks 5x5 dither pattern		
0.00	3.6	8.1
2.17	14.4	9.6
3.07	14.4	6.7
4.34	14.4	1.7
4.85	28.8	1.0
6.14	14.4	0.0
90 ks hexagonal pattern		
0.00	12.9	15.3
2.00	77.1	23.2

[†] The somewhat ill-defined unit is here taken to use the source flux integrated over the energy interval from 3 to 10 keV relative to the Crab flux integrated over the same interval.